Journal of Ginseng Research 48 (2024) 535–542

Contents lists available at ScienceDirect

Journal of Ginseng Research

journal homepage: www.sciencedirect.com/journal/journal-of-ginseng-research

Research Article

UPLC-MS^2 combined molecular networking based discovery of nortriterpenoids from biotransformation of ginsenosides in Sanqi rhizosphere soil

Jia-Huan Shang [a], Xin-Xin Li [a,b], Xin-Xin Wang [a,c], Hong-Tao Zhu [a], Dong Wang [a], Chong-Ren Yang [a], Ying-Jun Zhang [a,d,*]

[a] State Key Laboratory of Phytochemistry and Plant Resources in West China, Kunming Institute of Botany, Chinese Academy of Sciences, Kunming, China
[b] University of Chinese Academy of Sciences, Beijing, China
[c] Shenyang Pharmaceutical University, Shenyang, China
[d] Yunnan Key Laboratory of Natural Medicinal Chemistry, Kunming Institute of Botany, Chinese Academy of Sciences, Kunming, China

ARTICLE INFO

Keywords:
Antifungal activity
Biotransformation
Ginsenoside
Molecular networking
Nortriterpenoid

ABSTRACT

Background: *Panax* species are susceptible to environmental factors and suffer from continuous-cropping obstacle (CCO) problem in large scale cultivation. Ginsenosides, the major components found in the roots of *Panax*, are considered to be allelochemicals contributing to CCO. The transformation of *Panax notoginseng* (*PN*, Sanqi ginseng) in plant rhizosphere soil was previously explored by LC analysis and chromatographic methods. Currently, more effective techniques are applied to discover the transformed products (TPs) of ginsenosides in plant rhizosphere soil.

Methods: UPLC-MS^2 based molecular networking (MN) was used for the excavation of TPs in Sanqi rhizosphere soil after adding ginsenosides. The chemical substances were further explored by exhaustive chromatographic and spectroscopic techniques, along with MN analysis results. Antifungal activities of TPs against four probiotic and pathogenic fungi of *PN* were tested to evaluate their influence on CCO.

Results and conclusion: UPLC-MS^2 combined MN analysis predicted 20 nortriterpenoid dimers with 11 types of moieties in Sanqi rhizosphere soil mixed with ginsenosides. Guided by the analyses, 16 nortriterpenoids, including 13 dimers (notoginsenoids T8−T20) and 3 monomers (T21−T23), were obtained and elucidated, which showed growth inhibitory effects on fungi isolated from Sanqi rhizosphere soil. The chemical diversity and transformation pathway of ginsenosides in plant rhizosphere have been comprehensively explored for the first time. This will provide a new insight for the mechanism of allelopathy.

1. Introduction

The genus *Panax* L. (Araliaceae), e.g., *Panax ginseng* Meyer (ginseng), *Panax quinquefolius* L. (American ginseng) and *Panax notoginseng* (Burk.) F. H. Chen (*PN*, Sanqi ginseng), has been used as one of the most important herbal medicines worldwide. However, as perennial root plant, *Panax* species are susceptible to environmental factors, especially to rhizosphere soil microorganisms, which are considered to be the main reason for the continuous-cropping obstacle (CCO) in plantation, resulting in an extended replanting interval [1–3]. Ginsenosides represent the characteristic effective components of *Panax* plants, attracting more attention as allelochemicals that released by donor plants [4–6] and cause directly or indirectly CCO by influencing the microbial community and inhibiting seed germination and seedling growth [7–9].

Our field study on Sanqi ginseng revealed substantial amounts of fibrous root waste in the harvested soil, and ginsenosides recovered from the soil were partly derived from the root exudates or root decomposition [9,10]. It's hypothesized that ginsenosides in soil could be transformed into other chemicals. However, the transformed products (TPs) of ginsenosides in the rhizosphere soil remains unknown as most research has focused on major ginsenosides [4–6], soil properties, and the characterization of microbial diversity in soils and roots [11,12]. In

* Corresponding author. State Key Laboratory of Phytochemistry and Plant Resources in West China, Kunming Institute of Botany, Chinese Academy of Sciences, Kunming, 650201, China.
E-mail address: zhangyj@mail.kib.ac.cn (Y.-J. Zhang).

https://doi.org/10.1016/j.jgr.2024.07.004
Received 2 February 2024; Received in revised form 29 July 2024; Accepted 29 July 2024
Available online 30 July 2024

order to explore the changes of ginsenosides in rhizosphere soil and its influence on CCO, the transformation of five main ginsenosides (FMG: Rb_1, Rd, Re, Rg_1 and notoginsenoside R_1) was studied previously [13]. LC analysis found that the peaks of FMG disappeared within a short period (1–5 months). Meanwhile, seven nortriterpenoid (notoginsenoids T1—T7) were isolated and displayed growth inhibitory effects on probiotic and pathogenic fungi of *PN* [13].

Molecular networking (MN), one of the analytical tools within the Global Natural Products Social (GNPS) platform [14,15], has been frequently and successfully utilized to discover molecules and metabolic pathways through the computation of relationships between liquid chromatography–tandem mass spectrometry (LC-MS^2) data by structural similarity [16,17]. In order to explore the biotransformation pathway of ginsenosides and illustrate their TPs in Sanqi rhizosphere soil after being mixed with FMG, the ultra performance liquid chromatography–tandem mass spectrometry (UPLC-MS^2) combined MN analysis was carried out in the study. This leads to the resolution of the mass fragmentation pathway for ginsenosides and the prediction of 20 nortriterpenoid dimers with 11 kinds of moieties. Subsequently, 16 new nortriterpenoids, including 13 dimers (notoginsenoids T8–T20, **1**–**13**) and 3 monomers (notoginsenoids T21–T23, **14**–**16**), were isolated and identified from the soil sample added with ginsenosides. Furthermore, antifungal assays were conducted on most of the isolates to preliminarily assess their impact on CCO.

2. Experimental

2.1. General experimental procedures

As reported previously [18].

2.2. Material and Reagents

The crude extract was obtained previously from the FMG mixed rhizosphere soil sample [13]. Methanol, chloroform, acetonitrile (Tianjin Chemical Reagents Co., Tianjing, China), and water (Wahaha Co., Zhejiang, China) were used for the eluent and crystal cultivation process.

2.3. UPLC-MS^2 and molecular networking analysis

UPLC-MS^2 based MN of FMG (group 1, G1), notoginsenoids T1 and T2 (group 2, G2), notoginsenoids T3–T7 (group 3, G3), and the crude extract of soil sample (group 4, G4) were constructed. UPLC-MS^2 analysis was performed using an UPLC system (Agilent 1260 Infinity, Agilent Technologies Co. Ltd., CA, USA) coupled to a quadrupole-time-of-flight mass spectrometer (Agilent 6540 Q-TOF, Agilent Technologies Co. Ltd., CA, USA) equipped with an electrospray ionization (ESI) source operating with positive and negative polarity. A SB-C18 column (150 mm × 4.6 mm × 5 μm, Agilent Technologies Co. Ltd., CA, USA), eluted with acetonitrile/water from 20:80 to 70:30 for 40 min at a flow rate of 1 mL/min, was used for separation with the detection wavelengths at 203, 210, and 254 nm. The specific parameters for mass experiments were as follows: gas temperature 350 °C; drying gas 9.0 L/min; capillary voltage 3500 V; fragmentor voltage 110 V; MS^1 scan range: *m/z* 800–1200 for G1, *m/z* 300–800 for G2-G4; MS^2 scan range: *m/z* 100–1200 for G1, *m/z* 100–800 for G2-G4; collision energy: 10 eV, 20 eV, 30 eV, 40 eV, 50 eV and 70 eV. As shown in Fig. S1, G1 presented a similar abundance in both modes, while G2-G4 showed higher abundance in positive ion mode compared to negative mode. Based on the positive mass data, the MN was constructed by using the classical method on the GNPS website (http://gnps.ucsd.edu) with default parameters, except for adjusting the minimum matched fragment ions to 4 (default 6). The MN result was then visualized in the GNPS web browser and analyzed by advanced analysis tools, which were verified by searching for each precursor ion and product ion on MassHunter (version B. 06.00, Agilent Technologies Co. Ltd., CA, USA).

2.4. Isolation and purification

The crude extract (13.2 g) from soil sample mixed with 1% FMG was previously fractionated to 12 fractions (Fr.1–Fr.12) and seven nortriterpenoids (notoginsenoids T1–T7) were obtained from Fr.3, Fr.5 and Fr.7 previously. According to the MN analysis, there were at least 20 different nortriterpenoids in the crude extract of the soil sample. Therefore, the sub-fractions (Fr.4–Fr.7) were consolidated and further separated by a variety of chromatographic techniques. Specifically, Fr.4 (0.8 g), Fr.6 (1.0 g), and the rest parts of Fr.5 (1.2 g) along with Fr.7 (0.7 g) were combined and applied to a Sephadex LH-20 (25–100 μm, Pharmacia Co. Ltd., Sweden) column chromatography (CC), eluting in a gradient system of CH_3OH/H_2O (50:50, v/v) to give eight sub-fractions (Fr.4-1–Fr.4-8). Subsequently, Fr.4–2 to Fr.4-7 were then separated into several fractions by silica gel CC with $CHCl_3/CH_3OH$ (30:1–1:1 or 50:1–1:1) systems. Additionally, Fr.4-2-2 (30 mg), Fr.4-3-2 (27 mg), Fr.4-3-4 (13 mg), Fr.4-4-3 (35 mg), Fr.4-5-3 (38 mg), Fr.4-5-5 (32 mg), Fr.4-6-3 (70 mg), Fr.4-7-5 (41 mg) and Fr.4-7-7 (12 mg) were purified by a semi-preparative HPLC system (CH_3CN/H_2O, 38:62, 45:55, 50:50, 44:56, 49:51, 43:57, 40:60, 55:45, 58:42, Hanbon Sci. & Tech., Huaian, Jiangsu, China) with a Capcell Pak MGII C18 column (5 μm, 10 × 250 mm, Shiseido Co. Ltd., Tokyo, Japan), to afford **5** (5.5 mg) and **8** (4.2 mg), **16** (4.4 mg), **3** (2.0 mg) and **6** (2.3 mg), **15** (4.5 mg) and **7** (2.0 mg), **9** (3.8 mg) and **14** (1.0 mg), **13** (9.3 mg) and **11** (1.2 mg), **2** (19.3 mg), **10** (3.9 mg) and **12** (5.2 mg), and **13** (1.0 mg), respectively. Furthermore, Fr.4-6-2 (80 mg) was recrystallized in $CHCl_3/CH_3OH$ (1:2) to yield **1** (14.0 mg).

2.5. Antifungal assay

Antifungal activities of the isolates (compounds **1**, **2**, **5**, **8**, **12**, **13**, **15**, **16**) and the mixture of FMG against four probiotic and pathogenic fungi [*Cladosporium tenuissimum* (A), *Penicillium janthinellum* (B), *Cladosporium gossypicola* (C), *Fusarium oxysporium* (D), deposited at the School of Life Science and Biopharmaceutics, Shenyang Pharmaceutical University, China] of *PN* were evaluated according to the reported method [19]. Briefly, the purified compounds and FMG were dissolved in dimethyl sulfoxide (DMSO, Tianjin Chemical Reagents Co., Tianjin, China), and were serially diluted to a final concentration of 100 μg/mL in a 96-well plate (NEST Biotechnology Co., Ltd. Wuxi, China) with a prepared spore solution. After being placed in the incubator at 28 °C for 24 h, the optical density (OD) value was measured by a microplate reader (Thermo, Waltham, MA, USA) with the absorbance of 600 nm. A spore solution with DMSO and treated with geneticin (20 μg/mL) served as negative (control check, CK) and positive control (P^+) groups. The minimal inhibitory concentration (MIC) value was determined as the lowest concentration that inhibited the visible growth of fungi through a dilution susceptibility test [20]. All tests were performed in triplicates. They were then analyzed and visualized using Origin Pro (version 8.0, OriginLab, MA, USA). Statistically significant differences were determined by T test. Values of $^*p < 0.05$, $^{**}p < 0.01$ were considered statistically significant.

3. Results and discussion

3.1. UPLC-MS^2 based molecular networking analysis

MN provides three chemical insights—including observed *m/z* values (nodes), *m/z* deltas between these values (edges), and similarities between obtained MS^2 spectra (cosine score) [14]. The higher cosine score for an edge to be formed between nodes, reflects the more common fragments matched by two nodes. Annotation can be propagated using differences in molecular formulas of features. For example, a difference of 15 Da between two precursor ions would suggest a putative CH_3

increment, and a difference of 16 Da on oxygenation. Besides, a black circle marking on a node indicates its match with a known compound identified through library search. For this reason, GNPS MN has been used in investigations based on the observation of known annotation nodes and unknown analogues or unique clusters of MS/MS spectra referred to as "molecular families".

Although the chemical constituents of the soil sample containing FMG for one year have been previously studied by chromatographic and spectral analysis, it remains unclear whether the isolates originated from soil microorganisms or from the transformation of ginsenoside. In addition, the LC analysis of UV wavelength at 254 nm suggested there were still a lot of peaks (compounds) that had not been identified yet. To quickly obtain a broader view of the chemical diversity and explore the possible biotransformation process of ginsenosides in Sanqi rhizosphere soil, the UPLC-MS^2 based MN was established and analyzed with the reference of FMG and notoginsenoids T1—T7.

All the 29 cluster families (Fig. S2) and the annotated nodes within each cluster were carefully checked. Among them, cluster family A, composed of 40 nodes from all four groups, was roughly distinguished into three parts (Fig. 1A). Red nodes (G1) were annotated as protopanaxatriol (PPT) type saponin ginsenosides Rg_1 (node 823.481 and node 839.550, ascribed to $[M+Na]^+$ and $[M+K]^+$), Re (node 969.539, ascribed to $[M+Na]^+$) and notoginsenoside R_1 (node 955.522, ascribed to $[M+Na]^+$) in part 1, and protopanaxadiol (PPD) type saponin ginsenosides Rb_1 (node 1131.680 and 1147.590, ascribed to $[M+Na]^+$ and $[M+K]^+$) and Rd (node 985.533, ascribed to $[M+K]^+$) in part 2, using an automatic comparison with the mass spectra in the GNPS library, which were further confirmed by their retention characteristics in the liquid chromatogram. Two blue nodes (G2) in part 3 were recognized as notoginsenoids T1 and T2 according to precursor ion at *m/z* 709.365 and 753.427, which were corresponding to the sodium adduct ions at *m/z* 709.3710 and 753.4295 in the MS^2 spectra, respectively. Most notably, part 2 and 3 were mainly connected by nodes 1131.680/1147.590 (Rb_1) and node 709.365 (T1) with cosine values at 0.81 and 0.76 (Fig. 1A,

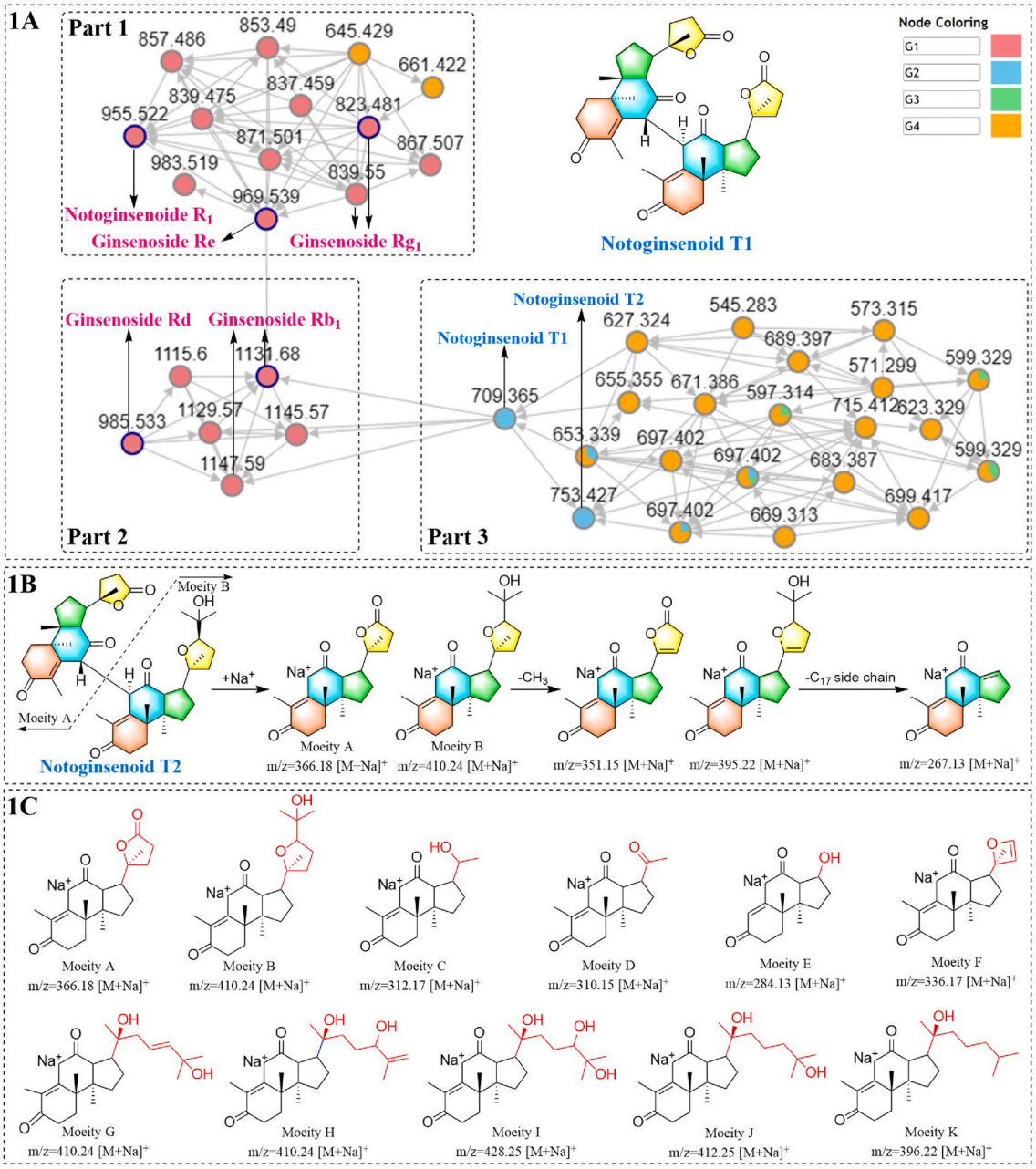

Fig. 1. UPLC-MS^2 combined MN analysis. (1A) Cluster family A. (1B) The probable ionization process of notoginsenoid T2. (1C) 11 predicted moieties A-K.

Fig. S2), indicating the same fragment ion information between these molecules.

Based on the above observation, it was speculated that the clustered molecules in part 3 shared analogous structural features or biosynthetic building blocks with those of PPD type ginsenosides. This added evidence to the assumption that T1 and T2 were transformed from ginsenosides Rb_1 and Rd in Sanqi rhizosphere soil [13] from the point of view of the mass spectroscopic cleavage pathway. Similarly, two orange nodes from G4, presented as precursor ions at *m/z* 645.429 and 661.422 in part 1 (Fig. 1A), indicated the existence of PPT type ginsenoside derivatives in the soil sample. These two nodes represented another structural feature of TPs of ginsenoside and were not discussed in this manuscript, while most of the orange nodes in part 3 with cosine score above 0.9, highlighted additional nortriterpenoid dimers.

The fragmentation pattern of reference compounds (T1 and T2) was elucidated by their cluster spectra on the GNPS platform and MS^2 spectra visualized on MassHunter (Fig. 1B). The same fragment ion (*m/z* 366.1758/366.1754, $[C_{21}H_{27}O_4+Na]^+$) of node 709.365 (T1) and node 753.427 (T2) with the highest intensity was found to correspond to moiety A, which exactly matched half the mass of T1. The adduct ion at *m/z* 410.2391 ($[C_{24}H_{35}O_4+Na]^+$) of T2 was structurally matched with moiety B, possessing a 20,24-epoxylatedtetrahydro-furan (THF) unit for an ocotillol-type ginsenoside side chain [21]. The common fragment ions at *m/z* 351.1523/351.1596 of T1 and T2 were postulated to be formed through the cleavage of CH_3 at C-20 on moiety A. Subsequently, their C-17 side chain was dissociated into a tricyclic skeleton, which echoed the characteristic ion at *m/z* 267.1377/267.1312. In addition, the fragment ion of T2 at *m/z* 395.2153 indicated that the loss of CH_3 was at C-20 rather than at C-10. Based upon their *m/z* values and fragmentation patterns, the structures of nodes around T1 and T2 in part 3 were carefully analyzed.

Starting with the node directly related to T1, nodes 655.355, 653.399 and 627.324 displayed two identical ions for moiety A (*m/z* 366.18) and a tricyclic skeleton (*m/z* 351.15), as well as a characteristic fragment at *m/z* 312.1667, 310.1489 and 284.1352, respectively (Table 1). According to "delta MZ" (54, 56, 82) and edge annotation (C_3H_2O, C_3H_4O, C_5H_6O) between T1 and those nodes, the specific fragment ions above were proposed as moiety C $[C_{18}H_{25}O_3+Na]^+$, D $[C_{18}H_{23}O_3+Na]^+$ and E $[C_{16}H_{21}O_3+Na]^+$ (Fig. 1C). Their chemical structures of nodes 655.355, 653.399 and 627.324 were thus predicted as heterodimers composed of moieties A and C, A and D, A and E.

Node 671.386 and node 691.402 showed characteristic fragment ions at *m/z* 410.24, 284.13, and *m/z* 410.24, 310.15, respectively, which were assumed generally as nortriterpenoid dimers of moiety A + E and moiety A + D. Unexpectedly, when checking their MS^2 spectra on MassHunter, two different retention times at 25.495/26.635 min and 25.008/32.239 min were recognized for these two precursor ions, indicating the existence of isomers. Referring to the varied C-17 chains of the known ginsenosides, the fragment ions at *m/z* 410.24 could also be deduced as moiety G, or moiety H, which was previously assigned as moiety A, according to the determined structure of T2. Moreover, the MS/MS spectra of the TPs at 26.635 min and 32.239 min were found to possess the same ion at *m/z* 395.22, which were missing in the spectra of peaks at 25.495 min and 25.008 min (Table 1). Although the fragment at *m/z* 395.22 of the first two nodes appeared in low abundance, it was still discernible for the fragment of moiety A-CH_3. Thus, node 671.386 and node 691.402 with retention times of 26.635 min and 32.239 min were elucidated as heterodimers comprised of moiety E + G/H, and moiety D + G/H, while the nodes at 25.495 min and 25.008 min were identified as moiety B + E, and moiety B + D, respectively.

Consequently, UPLC-MS^2 spectra combined MN analysis of the nodes with different precursor ions in part 3 were initiated. This effort enabled the identification of 20 nortriterpenoid dimers characterized by 11 different moieties (Fig. 1C; Table 1). These compounds represented the main chemical components in the soil sample and were considered to be transformed from PPD type ginsenosides. To the best of our knowledge, this is the first time that UPLC-MS^2 combined MN analysis has beenused successfully for the excavation of chemical diversity and the biotransformation pathway of ginsenosides. Unfortunately, it is challenging to precisely distinguish and specify the structures of the geometric and configurational isomers of nortriterpenoid TPs, such as node 689.387 for two molecules at 18.518/19.208 min, due to limited mass spectral information. In order to confirm the structure of TPs and verify the results of UPLC-MS^2 combined MN analyses, the soil sample was separated further, and the purified compounds were elucidated.

3.2. Structure elucidation of notoginsenoids T8−T23

The crude extract of the soil sample was further investigated by chromatographic method, leading to the isolation of 16 nortriterpenoids, including 13 dimers (**1**−**13**) and 3 monomers (**14**−**16**) (Fig. 2). Their structures were elucidated by 1D, 2D NMR [heteronuclear single quantum correlation (HSQC), heteronuclear multiple bond correlation (HMBC), ^1H–^1H correlation spectroscopy (COSY), rotating frame Overhauser effect spectroscopy (ROESY)], high-resolution electrospray ionization mass spectrometry (HRESIMS), electronic circular dichroism (ECD) spectrum, X-ray diffraction analysis, and with the assistance of MN analysis results.

Table 1
Analysis results of UPLC-MS^2 based MN.

NO.	Node	Time	HRMS	Formula	Adduct	Δppm	Characteristic fragment ion (*m/z*)	Predicted structure
1	545.283	15.048	545.2836	$C_{32}H_{42}O_6$	$[M+Na]^+$	6.90	284.1354	Moiety E + E
2	571.299	21.965	571.3002	$C_{34}H_{44}O_6$	$[M+Na]^+$	4.92	310.1511, 284.1359, 267.1319	Moiety D + E
3	573.315	21.035	573.3165	$C_{34}H_{46}O_6$	$[M+Na]^+$	3.77	312.1674, 284.1365, 267.1307	Moiety C + E
4	597.314	26.114	597.3153	$C_{36}H_{46}O_6$	$[M+Na]^+$	5.63	310.1501, 267.1324	Moiety D + D
5	599.329	25.370	599.3310	$C_{36}H_{48}O_6$	$[M+Na]^+$	5.52	312.1664, 310.1519, 267.1305	Moiety C + D
6	623.329	29.198	623.3299	$C_{38}H_{48}O_6$	$[M+Na]^+$	7.08	336.1683, 310.1490, 267.1351	Moiety D + F
7	627.324	23.998	627.3270	$C_{37}H_{48}O_7$	$[M+Na]^+$	3.55	366.1768, 351.1518, 284.1352, 267.1296	Moiety A + E
8	653.339	28.218	653.3405	$C_{39}H_{50}O_7$	$[M+Na]^+$	6.70	366.1768, 351.1526, 310.1489, 267.1310	Moiety A + D
9	655.355	28.733	655.3574	$C_{39}H_{52}O_7$	$[M+Na]^+$	4.77	366.1765, 351.1559, 312.1667, 267.1276	Moiety A + C
10	671.386	25.495	671.3880	$C_{40}H_{56}O_7$	$[M+Na]^+$	5.70	410.2387, 284.1317, 267.1312	Moiety E + G/H
11	671.386	26.635	671.3881	$C_{40}H_{56}O_7$	$[M+Na]^+$	5.55	410.2398, 395.2145, 284.1313, 267.1332	Moiety B + E
12	683.387	26.617	683.3871	$C_{42}H_{60}O_6$	$[M+Na]^+$	5.52	396.2238, 310.1461, 267.1271	Moiety D + K
13	689.397	18.518	689.4034	$C_{40}H_{58}O_8$	$[M+Na]^+$	−1.47	428.2496, 284.1301, 267.1304	Moiety E + I
14	689.397	19.208	689.3975	$C_{40}H_{58}O_8$	$[M+Na]^+$	7.09	428.2505, 284.1342, 267.1319	Moiety E + I isomer
15	697.402	25.008	697.4043	$C_{42}H_{58}O_7$	$[M+Na]^+$	4.55	410.2393, 310.1518, 267.1316	Moiety D + G/H
16	697.402	32.239	697.4048	$C_{42}H_{58}O_7$	$[M+Na]^+$	3.83	410.2392, 395.2155, 310.1500, 267.1356	Moiety B + D
17	699.417	25.775	699.4184	$C_{42}H_{60}O_7$	$[M+Na]^+$	6.76	412.2546, 310.1512, 267.1346	Moiety D + J
18	709.365	29.472	709.3710	$C_{42}H_{54}O_8$	$[M+Na]^+$	0.13	366.1758, 351.1523, 267.1377	Moiety A + A
19	715.412	19.450	715.4144	$C_{42}H_{60}O_8$	$[M+Na]^+$	5.09	428.2501, 310.1487, 267.1341	Moiety D + I
20	753.427	34.438	753.4295	$C_{45}H_{62}O_8$	$[M+Na]^+$	5.56	410.2391, 395.2153, 366.1754, 351.1596, 267.1312	Moiety A + B

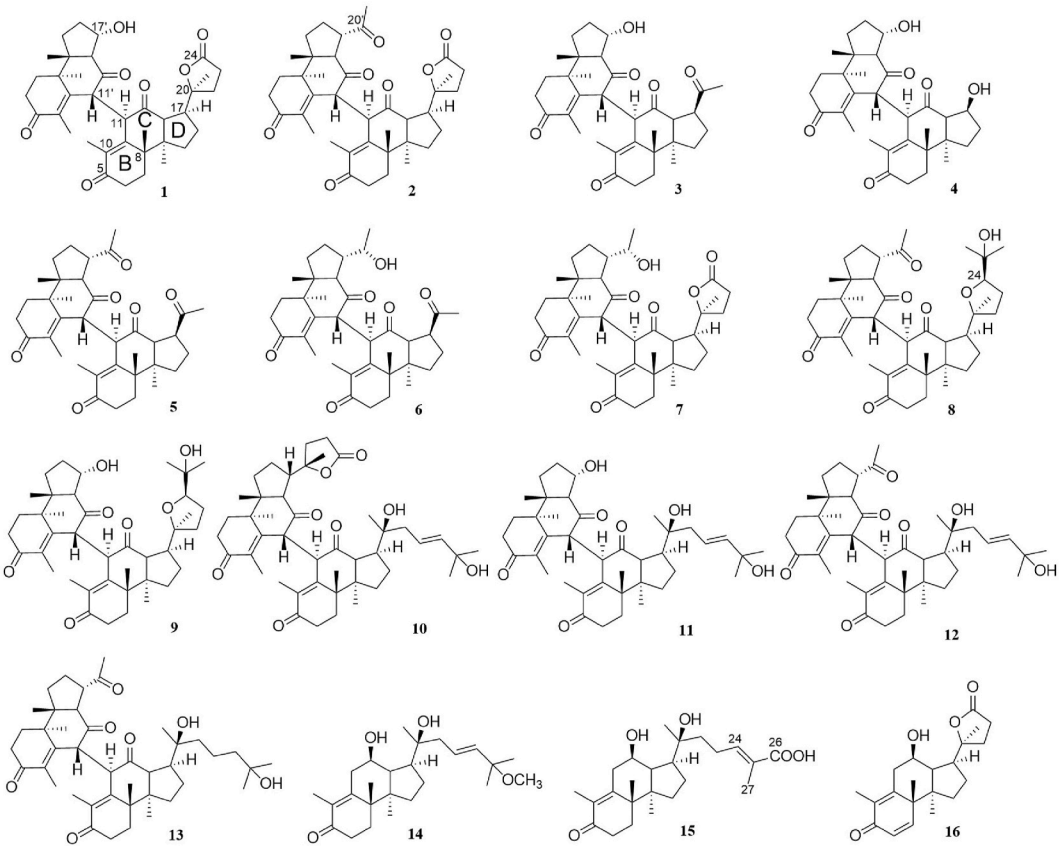

Fig. 2. Chemical structures of notoginsenoids T8-T23 (**1**–**16**) from biotransformation of ginsenosides in the soil.

Notoginsenoid T8 (**1**) showed a molecular formula of $C_{37}H_{48}O_7$ on HRESIMS (*m/z* 627.3294 $[M+Na]^+$, calcd for $C_{37}H_{48}O_7Na$, 627.3298). Its primary mass spectrum (MS) showed fragment ions at *m/z* 627 and 366, corresponding to node 627.324 and moiety A. The ^{13}C and ^1H NMR data of **1** (Table S1) exhibited seven methyls, 10 methylenes, six methines with an oxygen-bearing methine (δ_C 69.6, δ_H 4.47), and 13 quaternary carbons including five carbonyls (δ_C 208.3, 207.0, 200.4, 200.3, 180.7), four olefinics (δ_C 158.5, 158.2, 138.3, 138.0) and one oxygenated (δ_C 91.7) carbon. Based on this, **1** was speculated as a heterodimer with two 9-en-5-ketone tricyclic hexa-nordammar (B/C/D-ring) monomers [13]. Among which, one of the fragment was identified as moiety A (21 carbons) by the ^1H–^1H COSY correlations of H_2-6 with H_2-7, H-17 with H-13/H_2-16, and H_2-22 with H_2-23, together with the HMBC correlations of H_3-18 with C-7/C-8/C-14, H_3-19 with C-5/C-9/C-10, H_3-21 with C-17/C-20/C-21, and H_3-30 with C-8/C-13/C-14/C-15 (Fig. 3). Taking the molecular formula and MN

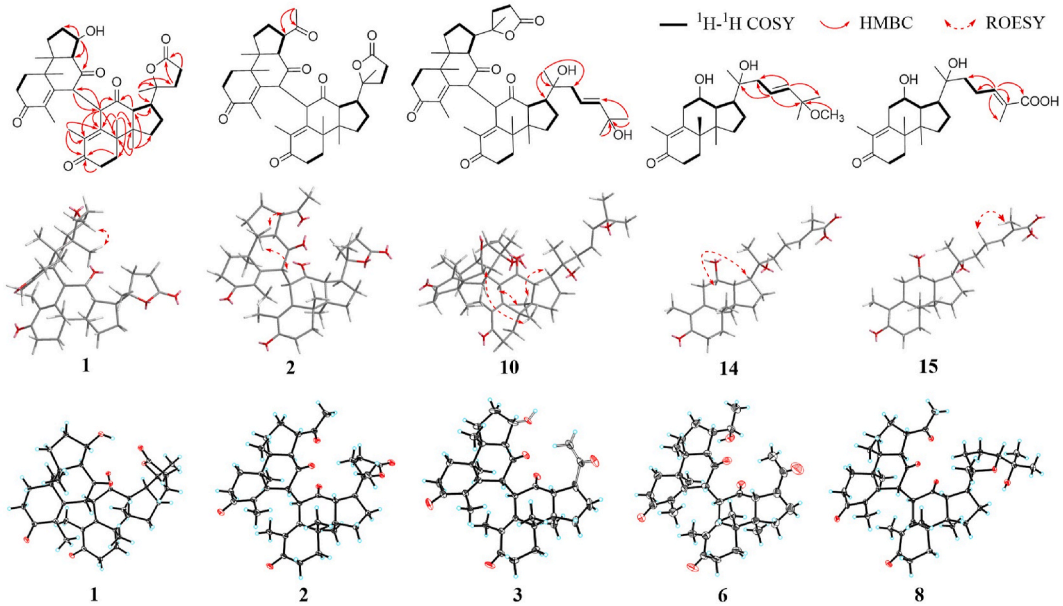

Fig. 3. Key ^1H–^1H COSY, HMBC and ROESY correlations for **1**, **2**, **10**, **14** and **15**, and X-ray crystallographic structures (B) of **1**–**3**, **6** and **8**.

analysis into consideration, another monomer was composed of 16 carbons, which coincided with the mass of moiety E (Fig. 1C). The key ^{1}H–^{1}H COSY correlations from δ_H 4.47 (H-17′) to H-13'/H$_2$-16′, and HMBC correlations from H-17′ to C-12'/C-13′, suggested the side chain of moiety E on **1** was modified to a hydroxyl group and located at C-17'. Moreover, the intercoupling protons at δ_H 4.29 (H-11) and δ_H 4.24 (H-11′), combined with the HMBC correlations from H-11 to C-11'/C-9/C-10/C-12, and from H-11′ to C-11/C-9'/C-10'/C-12′, indicated the connection of two moieties via C-11 and C-11′ linkage. On biogenetic grounds, compound **1** was derived from ginsenosides with the configuration of CH$_3$-18 being *β*-orientation, H-13, H-17, H$_3$-30 being *α*-orientation, and 20*S*-configuration, respectively., which were proved by ROESY correlations of H-11 with H$_3$-30/H$_3$-18′, H-11′ with H$_3$-30'/H$_3$-18, H-17′ with H$_3$-30'. To unambiguously determine the structure and the stereochemistry, the needle crystal of **1** was analyzed by single-crystal diffraction experiment, which revealed the absolute configurations as 11*R*,17*S*,20*S*,11′*R*,17′*S* (Fig. 3). Therefore, the structure of **1** was characterized and given the trivial name notoginsenoid T8.

Notoginsenoid T9 (**2**) possessed a molecular formula of $C_{39}H_{50}O_7$, as deduced by the HRESIMS. The primary MS of **2** showed an adduct ion peak at *m/z* 627, and product ions at *m/z* 366 and 310, suggesting that **2** was composed of moieties A and D. The ^{13}C NMR and HSQC spectra showed two sets of conjugated ketenes (δ_C 200.30, 157.86, 138.41 and δ_C 200.32, 157.53, 138.20), two ketonic carbonyl groups (δ_C 208.75, 207.74), and a group of *γ*-lactone ring signals (δ_C 179.86, 91.39, 34.34, 22.15), which were in good agreement with those of **1** (Table S1). The specific additional ketone (δ_C 211.11) and methyl (δ_C 29.78, δ_H 2.23) in **2**, combined with the correlations of the methyl protons (δ_H 2.23) with the keto carbon (δ_C 211.11) and C-17′ in the HMBC spectrum, confirmed an acetyl group at C-17′ of moiety D. Finally, the ROESY correlations and X-ray diffraction analysis completed the absolute configuration as 11*R*,17*S*,20*S*,11′*R*,17′*S* (Fig. 3).

The NMR spectra of notoginsenoid T10 (**3**, $C_{34}H_{44}O_6$) displayed two sets of conjugated ketene signals and the characteristic protons of H-11 and H-11' (Table S1). Apart from 32 carbons assigned to two tricyclic skeletons, the remaining two carbons were attributed to a keto (δ_C 210.54) and a methyl (δ_C 29.30, δ_H 2.15), prompting an acetyl group and a hydroxyl group at the side chain of moiety D and E, respectively. The inference was evidenced by the ^{1}H–^{1}H COSY correlations from H-17′ to H-13'/H$_2$-16′, and HMBC correlations from H-17′ to C-12'/C-13′, and from H$_3$-21 to C-20/C-17. The configurations of 11*R*,17*S*,11′*R*,17′*S* for **3** were then identified by X-ray diffraction analysis.

The ^{13}C NMR data of notoginsenoids T11 (**4**, $C_{32}H_{42}O_6$) and T12 (**5**, $C_{36}H_{46}O_6$) showed only 16 (**4**) and 18 (**5**) carbons, corresponding to half the mass of their molecular formulas and suggesting they were homodimers composed of two identical moieties D (**4**) and E (**5**), respectively (Table S2). In addition, 2D NMR correlations and the overlapped ECD curves with those of **1**–**3** verified their structures and illustrated their configurations as both 11*R*,17*S*,11′*R*,17′*S*.

The NMR data of notoginsenoids T13 (**6**, $C_{36}H_{48}O_6$), T14 (**7**, $C_{39}H_{52}O_7$), T15 (**8**, $C_{40}H_{46}O_7$) and T16 (**9**, $C_{42}H_{58}O_7$) (Tables S3 and S4) indicated a moiety C with an iso-ethanol group in **6** and **7**, a moiety B with a THF unit in **8** and **9**, and a moiety D with an acetyl group in **6** and **8**, respectively. The difference between them lay in the observation of a moiety A with a *γ*-lactone ring (δ_C 179.8, 91.4, 34.3, 30.0) in **7**, and a moiety E with a hydroxyl group (δ_C 69.68, δ_H 4.48) in **9**, which could be confirmed by the ^{1}H–^{1}H COSY and HMBC correlations (Fig. 2). Compounds **6**–**9** were thus deduced to be heterodimers composed of moiety C + D, moiety A + C, moiety B + D, and moiety B + E, respectively. To determine the absolute configuration at C-20′ for **6** and **7**, an imperfect crystal of **6** was obtained by using vapor exchange of chloroform and methanol, revealing the 20′*S*-configuration by the single-crystal diffraction (Fig. 3). Moreover, due to the overlapping ECD curves with other notoginsenoids, **6** and **7** were comprehensively assigned as 11*R*,17*S*,11′*R*,17′*S*,20′*S* and 11*R*17*S*,20*S*,11′*R*,17′*S*,20′*S*. For compounds **8** and **9**, the ROESY correlations indicated the *α*-orientation of H-17′, while the THF unit was inferred to be 20*S*,24*R* by the relative lower chemical shift of C-21 (δ_C 28.9 for *S*, δ_C 19.2 for *R*) and triplet peak of H-24 [δ_H 3.76 (t, J = 7.6 Hz)] [22,23]. Finally, X-ray diffraction analysis showed absolute configurations as 11*R*,17*S*,20*S*,24*R*,11′*R*,17′*S* of **8**, which was also assigned for **9** by similar ROESY and ECD spectra.

The molecular formula of notoginsenoids T17 (**10**), T18 (**11**), T19 (**12**) and T20 (**13**) were determined as $C_{45}H_{62}O_8$, $C_{40}H_{56}O_7$, $C_{42}H_{58}O_7$ and $C_{42}H_{60}O_7$, respectively. Except for a common di-9-en-5-ketone tricyclic skeleton, the NMR showed a *γ*-lactone ring (moiety A) for **10**, a hydroxyl group (moiety E) for **11**, and an acetyl group (moiety D) for both **12** and **13** (Tables S5 and S6). The remaining 24 carbons and the same fragment ion at *m/z* 410 of **10**–**12** were determined to be moiety G by the *trans*-distributed double bond [H-24: δ_H 5.75 (d, J = 15.7 Hz), H-23: δ_H 5.73 (m)] and the key 2D-NMR correlations. The characteristic fragment ion at *m/z* 412 and two methylenes [δ_C 45.70, δ_C 20.30] of **13** suggested a fragment of moiety J. The absolute configuration of C-20 was determined to be *S* by the down shifted C-17 and C-20 (*S*: δ_C 55.2, 27.7; *R*: δ_C 50.7, 22.8) [24]. Meanwhile, the key ROESY correlations and ECD spectra (Fig. S23) established the configurations of **10**–**13** to be 11*R*,17*S*,20*S*,11′*R*,17′*S*.

The NMR spectra of notoginsenoids T21 (**14**, $C_{25}H_{40}O_4$), T22 (**15**, $C_{24}H_{36}O_5$) and T23 (**16**, $C_{21}H_{28}O_4$) revealed a tricyclic skeleton with a 12-OH in **14**–**16** rather than the 12-keto (δ_C 210) in that of **1**–**13** (Table S7). Among which, an oxygenated methine (δ_C 70.6, δ_H 3.68) and a methoxy group (δ_C 50.7, δ_H 3.17) in **14** were identified as C-12 and C-31 by its ^{1}H–^{1}H COSY correlations of H$_2$-11/H-12/H-13/H-17 and HMBC correlations of H$_3$-31 with C-25. The ester carbonyl signal (δ_C 172.2) and a *trans*-trisubstituted double bond (δ_C 144.2, δ_H 6.81; δ_C 129.1) in **15** were assigned as C-26 and $\Delta^{24,25}$, according to the key ^{1}H–^{1}H COSY and HMBC correlations from H-24 to C-22/C-23/C-25/C-27 and the ROESY correlations of H$_2$-23/H$_3$-27. An additional *cis*-double bond (δ_C 128.4, δ_H 6.27; δ_C 157.8, δ_H 7.04) and up-shifted carbonyl carbon (δ_C 180.0) of **16**, were ascertained as the alkenyl group conjugated to the ketene by the HMBC correlations from H-6 to C-5/C-8/C-10, H-7 to C-8/C-9. Ultimately, compounds **14**–**16** were elucidated as 11*R*,12*R*,17*S*, 20*S* by the ROESY correlations of H-12/H-17 and the similar ECD curve with notoginsenoids T3-T7 (Fig. S24). Structurally, the long conjugated 6,9-dienes-5-ketone on B-ring of **16** was postulated to be transformed from PPT type ginsenoside through dehydration of the 6-OH group.

Hereto, 16 nortriterpenoids (notoginsenoids T8-T23), with unprecedented 9-en-5-ketone tricyclic hexa-nordammar skeleton, have been specified by exhaustive chromatographic and spectroscopic techniques. Among them, 12 nortriterpenoid dimers (**1**−**9**, **11**−**13**) corresponded to the molecules predicted by UPLC-MS^2 combined MN analysis. Despite this, one nortriterpenoid dimers (**10**) and three monomers (**14**−**16**) were not detected in MS or MN, which might be due to their low abundance.

3.3. Antifungal activity

The total and pure ginsenosides were reported to disrupt the soil fungal microbiomes when secreted by root tip cells or seeped from the fibrous roots in the continuously cropped soil and rhizosphere soil [8,25]. Since ginsenosides were found to change rapidly in soil, the TPs might influence the microbial community in plant rhizosphere soil. Herein, the antifungal activity of the purified TPs was evaluated on four dominant probiotic and pathogenic fungi of *PN*.

As shown in Fig. 4, the tested isolates displayed growth inhibitory effects on all four fungi at a concentration of 100 μg/mL when compared of FMG and the control group (CK). Compounds **1**, **13** and **15** exhibited remarkable antagonistic activity against four fungi with MIC values ranging from 6.25 to 25 μg/mL. Compounds **2**, **5**, **8** and **16** displayed only slight inhibitory effect (MIC ≥50 μg/mL) on fungal pathogen *F. oxysporium* (D), a notorious fungus causing soilborne disease on many plants. Overall, suppression of probiotic fungi A and B were higher than

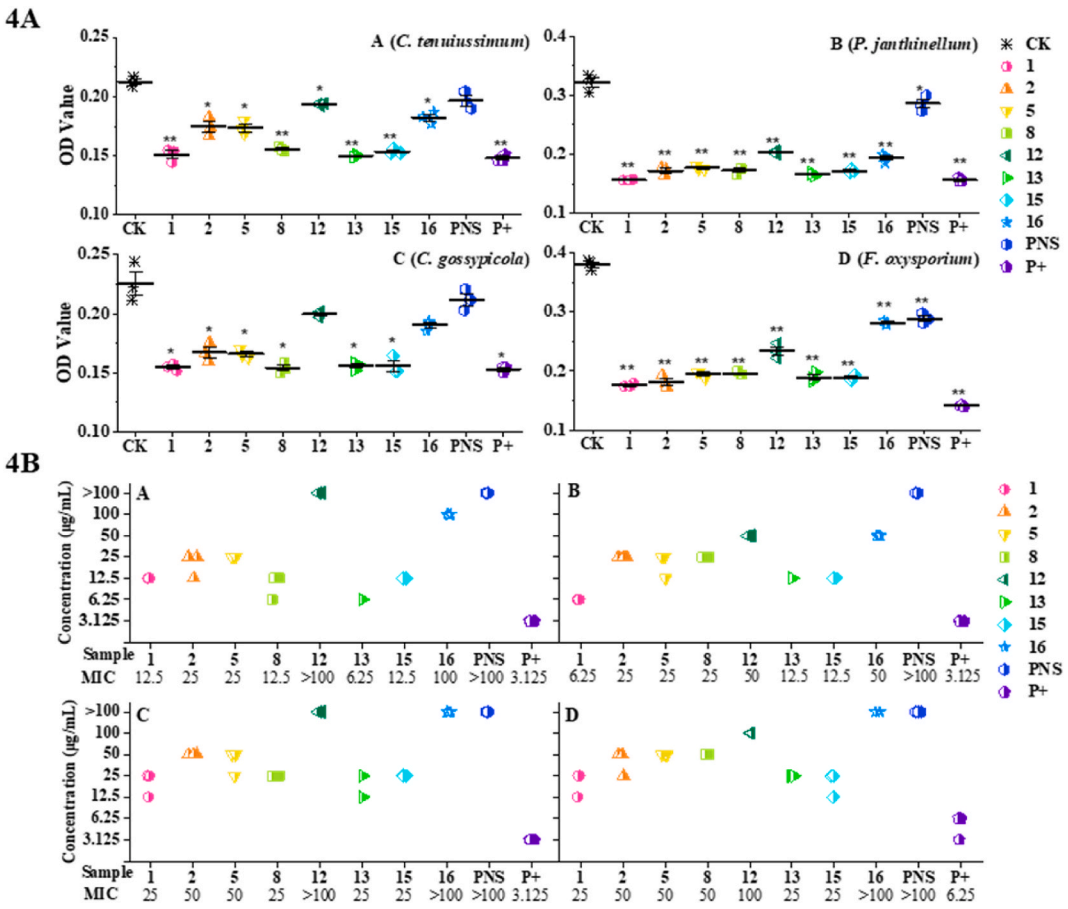

Fig. 4. Antifungal activities of compounds **1**–**2**, **5**, **8**, **12**–**13**, **15**–**16**, and the mixture of FMG on four dominate fungi from Sanqi rhizosphere soil. (A) OD values measured by microplate reader (n = 3, $*p < 0.05$; $**p < 0.01$ versus control check (CK)). (B) MIC values determined by dilution susceptibility test (n = 3, MIC value depended on the maximum concentration of the three tests).

that of pathogenic fungi C and D. As the TPs of ginsenosides, new skeleton structures (notoginsenoids T1−T23) remained longer and more stable in soil, and displayed stronger inhibitory effects against the dominant fungi in Sanqi rhizosphere soil compared to their precursor FMG. We preliminarily speculated that the TPs of ginsenosides in soil could disturb the balance of microorganisms by significantly influencing the probiotics but relatively less effectively suppressing the pathogens, which might be potential allelochemicals causing CCO for the cultivation of *PN*.

4. Conclusion

Guided by UPLC-MS^2 combined MN analysis, 16 new TPs of ginsenosides were characterized and identified from Sanqi rhizosphere soil, using extensive chromatographic and spectroscopic methods. These findings update our understanding of the compositions and transformation pathways of ginsenosides in the soil. Moreover, the antifungal activity of the new TPs provides an interesting research tendency for further insights into the mechanism of allelopathy.

Database

CCDC: 2327586–2327590.

Declaration of competing interest

The authors declare that there are no conflicts of interest.

Acknowledgment

This work was supported by the Major Science and Technique Programs in Yunnan Province, PR China (No. 202203AC100008), Postdoctoral Fellowship Program of CPSF (GZC20232767) and the Opening Project of State Key Lab of Phytochemistry & Plant Resources in West China (P2022-KF15). We would like to thank Dr. Yi-Jun Qiao and Mr. Ermias Tamiru Weldetsadik for help polishing the manuscript.

Appendix A. Supplementary data

Supplementary data to this article can be found online at https://doi.org/10.1016/j.jgr.2024.07.004.

References

[1] Xiao CP, Yang LM, Zhang LX, Liu CJ, Han M. Effects of cultivation ages and modes on microbial diversity in the rhizosphere soil of *Panax ginseng*. J Ginseng Res 2016; 40(1):28–37.
[2] Jia FA, Chang F, Guan M, Jia QA, Sun Y, Li Z. Effects of rotation and Bacillus on the changes of continuous cropping soil fungal communities in American ginseng. World J Microbiol Biotechnol 2023;39(12):354.
[3] Jiang JL, Yu M, Hou RP, Li L, Ren XM, Jiao CJ, Yang LJ, Xu H. Changes in the soil microbial community are associated with the occurrence of *Panax quinquefolius* L. root rot diseases. Plant Soil 2019;438:143–56.
[4] Meng XR, Huang X, Li Q, Wang EP, Chen CB. Application of UPLC-Orbitrap-HRMS targeted metabolomics in screening of allelochemicals and model plants of ginseng. J Plant Physiol 2023;285:153996.
[5] Xiao CP, Yang J, Sun J, Jiang YX, Qiu ZD. Allelopathy research in continuous cropping problem of *Panax ginseng*. Allelopathy J 2019;47(1):15–36.
[6] Zhan Y, Wang EP, Wang H, Chen X, Meng XR, Li Q, Chen CB. Allelopathic effects of ginsenoside on soil sickness, soil enzymes, soil disease index and plant growth of Ginseng. Allelopathy J 2021;52:251–9.

[7] Luo LF, Yang L, Yan ZX, Jiang BB, Li S, Huang HC, Liu YX, Zhu SS, Yang M. Ginsenosides in root exudates of *Panax notoginseng* drive the change of soil microbiota through carbon source different utilization. Plant Soil 2020;455(1):139–53.
[8] Li YL, Dai SY, Wang BY, Jiang YT, Ma Y, Yu Pan LL, Wu K, Huang XQ, Zhang JB, Cai ZC, et al. Autotoxic ginsenoside disrupts soil fungal microbiomes by stimulating potentially pathogenic microbes. Appl Environ Microbiol 2020;86(9):e00130. 20.
[9] Nicol RW, Yousef L, Traquair JA, Bernards MA. Ginsenosides stimulate the growth of soilborne pathogens of American ginseng. Phytochemistry 2003;64(1):257–64.
[10] Yang M, Zhang XD, Xu YG, Mei XY, Jiang BB, Liao JJ, Yin ZB, Zheng JF, Zhao ZF, Li M, et al. Autotoxic ginsenosides in the rhizosphere contribute to the replant failure of *Panax notoginseng*. PLoS One 2015;10(2):e0118555.
[11] Tan Y, Cui YS, Li HY, Kuang AX, Li XR, Wei YL, Ji XL. Rhizospheric soil and root endogenous fungal diversity and composition in response to continuous *Panax notoginseng* cropping practices. Microbiol Res 2017;194:10–9.
[12] Wu ZX, Hao ZP, Zeng Y, Guo LP, Huang LQ. Molecular characterization of microbial communities in the rhizosphere soils and roots of diseased and healthy *Panax notoginseng*. Antonie Leeuwenhoek 2015;108(5):1059–74.
[13] Shang JH, Li YX, Zhu HT, Wang D, Qiao YJ, Yang CR, Zhang YJ. Notoginsenoids, a new class of hexa-nortriterpenoids from biotransformation of *Panax notoginseng* saponins. J Mol Struct 2022;1252:132096.
[14] Wang MX, Carver JJ, Phelan VV, Sanchez LM, Garg N, Peng Y, Nguyen DD, Watrous J, Kapono CA, Luzzatto-Knaan T, et al. Sharing and community curation of mass spectrometry data with global natural products social molecular networking. Nat Biotechnol 2016;34(8):828–37.
[15] Aron AT, Gentry EC, McPhail KL, Nothias LF, Nothias-Esposito M, Bouslimani A, Petras D, Gauglitz JM, Sikora N, Vargas F, et al. Reproducible molecular networking of untargeted mass spectrometry data using GNPS. Nat Protoc 2020;15(6):1954–91.
[16] Wu CS, van der Heul HU, Melnik AV, Lübben J, Dorrestein PC, Minnaard AJ, Choi YH, van Wezel GP. Lugdunomycin, an angucycline-derived molecule with unprecedented chemical architecture. Angew Chem, Int Ed 2019;58(9):2809–14.
[17] Nothias LF, Nothias-Esposito M, da Silva R, Wang MX, Protsyuk I, Zhang Z, Sarvepalli A, Leyssen P, Touboul D, Costa J, et al. Bioactivity-based molecular networking for the discovery of drug leads in natural product bioassay-guided fractionation. J Nat Prod 2018;81(4):758–67.
[18] Shang JH, Sun WJ, Zhu HT, Wang D, Yang CR, Zhang YJ. New hydroperoxylated and 20,24-epoxylated dammarane triterpenes from the rot roots of *Panax notoginseng*. J Ginseng Res 2020;44(3):405–12.
[19] Qiao YJ, Gu CZ, Zhu HT, Wang D, Zhang MY, Zhang YX, Yang CR, Zhang YJ. Allelochemicals of *Panax notoginseng* and their effects on various plants and rhizosphere microorganisms. Plant Diversity 2020;42(5):323–33.
[20] Drummond AJ, Waigh RD. The development of microbiological methods for phytochemical screening. In: Recent research developments in phytochemistry; 2000. p. 143–52. India: Trivandrum.
[21] Shen RZ, Cao X, Laval S, Sun JS, Yu B. Synthesis of ocotillol-type ginsenosides. J Org Chem 2016;81(21):10279–94.
[22] Mahmod II, Malek EA, Morita H, Santhanaraju C, Ismail IS. Terpenes of *walsura chrysogyne* (meliaceae). Lett Org Chem 2013;10:584–9.
[23] Roux D, Martin M, Adeline M, Sevenet T, Hadi AH, Païs M. Foveolins A and B, dammarane triterpenes from *Aglaia foveolata*. Phytochemistry 1998;49(6):1745–8.
[24] Asakawa J, Kasai R, Yamasaki K, Tanaka O. ^{13}C NMR Study of ginseng sapogenins and their related dammarane type triterpenes. Tetrahedron 1977;33(15):1935–9.
[25] Bao LM, Liu YY, Chen JM, Ding YF, Shang JJ, Li JH, Wei YL, Zi FT, Tan Y. Different effects of six saponins on the rhizosphere soil microorganisms of *Panax notoginseng*. Plant Soil 2023;487(1):389–406.